Research Article

Govindaswamy Sundaramali*, Jeeva P. Aiyasamy, Sambantham Karthikeyan, Thanjavur K. Kandavel, Balasubramanian Arulmurugan, Sivanraju Rajkumar, Shubham Sharma*, Changhe Li, Shashi Prakash Dwivedi, Abhinav Kumar*, Rajesh Singh, and Sayed M. Eldin*

Experimental investigations of electrodeposited Zn-Ni, Zn-Co, and Ni-Cr-Co-based novel coatings on AA7075 substrate to ameliorate the mechanical, abrasion, morphological, and corrosion properties for automotive applications

https://doi.org/10.1515/rams-2022-0324 received December 05, 2022; accepted May 07, 2023

Abstract: The aluminum (Al) alloy AA7075 is widely used in various industries due to its high strength-to-weight ratio,

* Corresponding author: Govindaswamy Sundaramali, School of Mechanical Engineering, Vellore Institute of Technology, 632014, Tamil Nadu, India, e-mail: sundaramali.q@vit.ac.in

- * Corresponding author: Shubham Sharma, Department of Mechanical Engnieering, University Centre for Research and Development (UCRD), Chandigarh University, Mohali, India; School of Mechanical and Automotive Engineering, Qingdao University of Technology, 266520, Qingdao, China, e-mail: shubhamsharmacsirclri@gmail.com, shubham543sharma@gmail.com
- * Corresponding author: Abhinav Kumar, Department of Nuclear and Renewable Energy, Ural Federal University Named After the First President of Russia, Boris Yeltsin, 19 Mira Street, 620002, Ekaterinburg, Russia, e-mail: drabhinav@ieee.org
- * Corresponding author: Sayed M. Eldin, Faculty of Engineering, Centre for Research, Future University in Egypt, New Cairo 11835, Egypt, e-mail: elsayed.tageldin@fue.edu.eg

Jeeva P. Aiyasamy: School of Mechanical Engineering, Vellore Institute of Technology, 632014, Tamil Nadu, India, e-mail: pajeeva@vit.ac.in Sambantham Karthikeyan: School of Advanced Sciences, Vellore Institute of Technology, 632014, Tamil Nadu, India, e-mail: skarthikeyanphd@vit.ac.in

Thanjavur K. Kandavel: School of Mechanical Engineering, SASTRA Deemed to be University, Tirumalaisamudram, Thanjavur 613401, Tamil Nadu, India, e-mail: tkkandavel02@mech.sastra.edu

Balasubramanian Arulmurugan: Department of Mechanical Engineering, KPR Institute of Engineering and Technology, Coimbatore 641407, Tamil Nadu, India, e-mail: enggarul@gmail.com

Sivanraju Rajkumar: Department of Mechanical Engineering, Faculty of Manufacturing, Institute of Technology, Hawassa University, Hawassa, Ethiopia, e-mail: ccetraj@qmail.com

Changhe Li: School of Mechanical and Automotive Engineering, Qingdao University of Technology, 266520, Qingdao, China, e-mail: sy_lichanghe@163.com

which is comparable and replaceable to steel in many applications. However, it has poor resistance to wear and corrosion compared to other Al alloys. The conventional pressure die coating with Cr and cadmium has led to premature failure while the load is applied. It is indeed to develop a novel coating method to improve the mechanical, wear, and corrosion properties of AA7075 Al alloy. In the present investigation, the binary and ternary metals such as zinc-nickel (Zn-Ni), zinc-cobalt (Zn-Co), and nickelchromium-cobalt (Ni-Cr-Co) are electroplated on the substrate material (AA7075). In order to ensure optimal coating adhesion, the surface of the substrate material was pre-treated with laser surface treatment (LST). The mechanical and corrosion studies have been carried out on the uncoated and coated materials. It is observed from the findings that the ternary coating has higher wear resistance than the binary-coated material. The ternary coating has 64% higher resistance in the non-heat-treated status and 67% higher resistance in the heat-treated condition compared to the uncoated specimens. The tensile strength (MPa) of Ni–Cr–Co on AA7075 pressure die casting (PDC) is higher than the other deposits (582.24 of Ni-Cr-Co > 566.07 of Zn-Co > 560.05 of Zn-Ni > 553.64 of uncoated condition). The presence of a crystalline structure with the high alignment of Co and Ni atoms could significantly improve the corrosion resistance of Ni-Cr-Co coatings on AA 7075 PDC substrates when compared to binary coatings. The scanning

Shashi Prakash Dwivedi: G.L. Bajaj Institute of Technology &; Management, Greater Noida, Gautam Buddha Nagar, U.P. 201310, India, e-mail: spdglb@gmail.com

Rajesh Singh: Uttaranchal Institute of Technology, Uttaranchal University, Dehradun 248007, India; Department of Project Management, Universidad Internacional Iberoamericana, Campeche C.P. 24560, Mexico, e-mail: drrajeshsingh004@gmail.com

electron microscopy (SEM) images, X-ray diffraction (XRD), and X-ray photoelectron spectroscopy findings on the coated materials have been corroborated with the analyses on mechanical and corrosion properties. The XRD analysis of the Zn-Ni binary coating has reported that the diffraction peaks of y-NiZn₃ (831), y -Ni₂Zn₁₁ (330), and 631 with 2θ values 38, 43, and 73° are confirming the presence of Zn-Ni binary deposit on AA7075 PDC substrate. The XRD pattern of Zn-Cocoated material has revealed that the presence of three strong peaks such as Zn (110), Co (111), and CoZn (211) and two feeble peaks such as ε-CoZn₃ (220) and ε-CoZn₃ (301) are clearly visible. The XRD pattern of Ni-Cr-Co ternary coating has exhibited that the Ni-Cr-Co ternary deposit is a solid solution with a body-centered cubic structure due to the formation peaks at lattice plane such as (110), (220), and (210) with a crystal lattice constant of 2.88 A°. The SEM image for both the binary- and ternary-coated materials has exhibited that the deposited surface has displayed many shallow pits due to hitting by progressive particles. The SEM image has illustrated the presence of Zn-Ni atoms with smaller globular structure. The surface morphology of binary Zn-Co coating on the PDC AA7075 substrate has unveiled the evenly distributed dot-like structure and submerged Co particles in the galaxy of Zn atoms. To understand the effectiveness of bonding by laser texturing, cross-section SEM has been carried out which furthermore revealed the effective adhesion of Ni-Cr-Co on AA7075 PDC; this could also be the reason for the enhancement of microhardness, wear, and corrosion resistance of the said coating.

Keywords: electro-deposition, AA7075, micro-hardness, corrosion, tensile strength, wear

1 Introduction

Aluminum (Al) alloys are versatile, less expensive, and widely used materials. They are relatively light, highly ductile, and can be easily formed into thin foils for wrapping in many engineering applications [1]. Significant improvement was achieved in the mechanical properties of the advanced 2xxx and 7xxx series Al alloys due to continuous research [2]. Though the alloys find their applications in a wide spectrum of industries, they face many limitations and at times fail prematurely. Some of the reasons for premature failure are (a) the lack of required properties in metal alloys (low hardness, low melting point susceptible to stress corrosion cracking) [3], (b) the adverse effect of alloying elements [4], (c) the residual stresses, porosity, and dendritic structure of cast products (the defects that are formed during the manufacturing processes) [5], and

(d) the cracks caused by residual stresses or cold shuts in the component during solidification and cooling [6]. Porosity is a severe defect found commonly in pressure die casting (PDC) due to turbulence in injected molten metal and poses a severe problem in the case of pressure vessels as well as structural members [7].

The formation of porosity is due to two common reasons. They are shrinkage during solidification and gas or air entrapment due to the material-processing environment [8]. The life span of Al alloy parts can be extended by coating techniques, which enhance their mechanical properties and corrosion resistance properties [9]. Hydrogen embrittlement is a common defect in the Zn-based alloy electrodeposition [10]. This leads to deterioration in mechanical properties of coated material and causes stress corrosion cracking [11]. Electrodeposition on Al decreases wear to the possible extent. But for better results, reinforcement of microsized metallic or non-metallic particles in metal plating can be adopted successfully [12]. The co-deposition of homogeneous micro-size particles is not practical because the tendency of micro-particles to get agglomerated is very high [13]. Nonhomogeneous electro co-deposition results in the reduced wear resistance of the coated substrate. Hence, thorough research is needed to obtain uniform reinforced particle distribution with non-agglomeration conditions, which makes the coatings harder and more wear-resistant. Direct current (DC) is usually applied in coating processes [14].

Only a few research works have been carried out to find the influence of pulsed current on electro co-deposition. Both DC and alternating current parameters should be analyzed and kept under control to achieve maximum thickness and homogeneity in distribution and to find the suitability of the electrodeposition method. By sediment codeposition method, Ni with Al particles was deposited on AA 7072, and the adhesive strength of the coatings was estimated by adhesion test [15]. The chemical and phase compositions and surface morphology are independent of current density in the case of zinc-nickel (Zn-Ni) coating on austenitic steel [16]. The Zn-Ni coating is a substitute for cadmium coating as it is highly toxic. The conditions for the occurrence of normal or anomalous co-deposition accompanied by the enrichment of Ni or Zn were determined from the results obtained in a study of the influence exerted by the solution composition of co-deposited metals. The process parameters selected for the study were the potential difference, current density, deposition rate, and Zn-Ni film's chemical composition. It has opened up the opportunities for varying the Ni content in the coatings from less than 2 to 90% [17]. The alloy of 0.1% C and 13% Cr stainless steel has the maximum anti-pitting properties in the corrosion mechanism when comparing various

coatings [18]. Researchers found that the coatings of stainless steel were found to be more stressed than Cr coatings. Further, the thickness of the coating is directly proportional to the duration of plating and it decreases with gap distance. The dependency of these parameters leads to optimizing the electrode gap for maximum coating thickness [19]. The need for a material or coating with higher corrosion resistance and a lesser production cost led researchers to develop a new type of protective coating on metal, adhering to the present strict pollution regulations. Zn-Ni alloy coating of various compositions and different thicknesses on steel with both chromated and non-chromated conditions was done and examined. It is found from the results that the salt spray alloy coating of 15–18% Ni replaces the deposit of Zn and cadmium [20].

Li et al. investigated Al-graphene composite coatings prepared from the organic solvent solution system of AlCl₃ and LiAlH₄ dissolved in tetrahydrofuran by electrodeposition technique. They have reported that the mechanical properties of the Al-graphene composite coating on Al matrix have improved four times than the pure Al coating, which are attributed to the prominent mechanical strength and self-lubrication effects of graphene [21].

The electroplating of Ni–Cr and Ni–Cr–SiC depositions was developed on aircraft parts to improve the resistance to wear and corrosion properties [22]. The agglomeration of silicon carbide (SiC) in the Ni-Cr electroplating process has led to a porous structure in the coating that causes the failure of AA7075 PDC when a high load is applied. The aircraft AA7075 PDC components subjected to the saltwater environment were degraded by aggressive corrosion reaction with the corrosive medium [22]. The uncoated AA7075 PDC has high internal stress, which is vulnerable to the tensile strength and corrosion resistance of Al alloys [23]. It is imperative to develop surface coatings as an alternative to Ni-Cr and Ni-Cr-SiC deposition on AA7075 PDC that can be used in aircraft PDC Al alloy parts with less porosity [24].

It was found that the corrosion behavior of the Zn-Ni alloy coating was affected by the addition of Ni content from 10 to 25 g/L in step 5 of the study by Farooq et al. [25]. As a result of adding 25 g/L Ni to the Zn-Ni alloy coating, the corrosion rate decreased approximately four times, indicating that the Zn-Ni coating is behaving as a sacrificial dissolving agent.

Using chronoamperometry, impedance spectroscopy, and electron microscopy, the microstructural evolution of the Zn-Ni coatings in moderately alkaline NaCl solution under slightly anodic polarization can be studied. Vucko et al. reported that the tensile stress release due to Zn dissolution quickly led to the development of a mud-crack pattern in the coating, enabling oxygen reduction reaction to occur on the substrate [26].

Crasta and Shetty explored the effects of NaF additive concentration and treatment time on trivalent chromate coating, which has been developed as an alternative to hexavalent chromate coating; NaF additive concentration enhances the rate of film formation and decreases the corrosion rate [27].

Bae et al. studied the effect of the epichlorohydrin and imidazole (EI) polymer on the deposition behavior of the Zn-Ni alloy and found that the EI polymer decreases the transition current density due to the suppression of both Zn and Ni depositions thus causing the corrosion potential to shift to a noble direction [28].

Laser surface texturing (LST) is one of the promising techniques to create surface roughness for better bonding adhesive strength [29]. LST is an inexpensive, highly flexible, and suitable absorption-type wavelength made by "CETAC LSX-200" and is well suited for surface texturing [30].

It has been evident that Zn has better wettability characteristics, thus improving interfacial bonding characteristics between the coating and the substrate, thereby increasing "mechanical strength," "corrosion resistance," and "tribological characteristics." As Zn has improved "wettability characteristics," it is advisable to use hard materials as "secondary-phase materials" in "composite coatings" (e.g., "carbides": "silicon carbide" and "tungsten carbide"; "oxides": "iron oxide," "zirconium dioxide," "aluminum oxide," "titanium dioxide," and "silicon dioxide"). These materials provide remarkable "hardness," "corrosion resistance," "wear resistance," and "high-temperature oxidation resistance" for a wide range of industrial components [31-33].

Al, which is commonly used in aerospace applications due to its corrosion resistance, does not possess an adequate wear resistance on its own. In practical applications, it is therefore necessary to improve the surface properties. The characteristics of Zn make it an excellent corrosionresistant coating material. Zn coatings offer excellent field performance due to their ability to form thick, adherent corrosion films and a corrosion rate that is significantly lower than those of ferrous materials [34]. PVD magnetron sputtering technique was used to coat "titanium nitride (TiN)" on "aerospace Al7075-T6" in various circumstances. It was found that the hardness of TiN-coated specimens exceeded 720 HV, compared to only 170 HV for uncoated specimens [35]. A significant increase in fatigue life is observed in coated specimens as a result of the presence of residual compressive stresses. As a result, fatigue strength was improved by as much as 30% [36]. The fatigue strength of deposited materials is strongly influenced by the processing parameters and the deposit material. A Taguchi optimization method has shown improvements in surface hardness, adhesion, and surface roughness for coated samples [37]. Several research works suggest that coated specimens have an improved fatigue life when compared to uncoated specimens. In the aerospace and automobile industries, particularly where human safety is involved, fracture-based designs are most reliable and useful. Additionally, they are helpful for estimating the component's life span. As a result of the addition of Zn to Al, a heat treatable alloy with the highest strength can be produced, which is suitable for structural applications.

No significant reports could be found to obtain the surface finish for AA7075 PDC with improved mechanical properties that cater to the bulk properties of AA7075 PDC. The formation of the dendritic structure during solidification leads to deterioration in the mechanical properties of AA7075 PDC. The reason behind the selection of AA7075 PDC is to study the improvement of its performance in automotive and aircraft applications. The AA7075 highstrength Al alloy has many attractive properties such as low cost and high machinability and is most commonly used in aircraft structures. The alloying elements Zn, Cu, and Mg deteriorate corrosion resistance, thereby decreasing the life of aircraft structures. It is a well-known fact that during a typical aircraft operation, an aircraft is exposed to diverse environments owing to humid air, rain, heat, oil and hydraulic fluids, and seawater. Although the thickness of the deposition was found to be above 200 µm. As a result of the agglomeration of SiC during the electroplating process, Ni-Cr also becomes aggregated. When a high load is applied to Al-7075 PDC, a porous structure is formed within the coating. This leads to failure of the coating when a high load is applied. In order to address the aforementioned problems, the present investigation fulfills the research gap and finds a suitable solution. The present research work is focused to develop a novel electrodeposition of binary and ternary coatings by LST on AA7075 PDC material for the enhancement of hardness and tensile strength and wear and corrosion resistance of substrate material to lengthen the life span of AA7075 in actual applications. The optimized parameters have been used for the surface coatings on AA7075 PDC in the present study.

2 Materials and methods

The Al alloy AA7075 (Al-5.8Zn-2.4Mg-1.5Cu-0.24Fe-0.2Cr) has been used as a substrate material in the present investigation [1,15,35,37]. The thickness of 60 μ m is maintained for all the coatings and specimens subjected to various tests,

which is the requirement for industrial applications. LST of substrate material was used for electrodeposition of coatings on AA7075 alloy. It is a known fact that the LST method of coating improves the adhesion of coating material with the substrate material. LST has promisingly improved the hardness, tensile strength, and resistance to wear and corrosion also. A suitable absorption-type wavelength created by the CETAC LSX-200 equipment was used for the LST, as it is inexpensive and highly flexible. Argon gas has been used as a shielding gas during the laser exposure. A pulsed laser with an optimized parameter of 1,064 mm wavelength capable of developing pulses of 25 ns at 309 µm with a focal length of 550 mm had been used to create a slit of the rectangular shape of $18 \times 5 \,\mathrm{mm}^2$. Both binary and ternary coatings were applied using electrodeposition on the LST-created surface of the substrate material. The scanning electron microscopy (SEM) image of the surface of substrate material after the application of LST is shown in Figure 1.

Zn–Ni and zinc–cobalt (Zn–Co) binary coatings were considered for the present work. Nickel–chromium–cobalt (Ni–Cr–Co ternary coating was also used and compared for novel coating methods. The plating parameters that affect the quality of electrodeposits such as pH and temperature of electrolyte bath, current density, duration of the plating process, brightener, and additives were optimized for the deposition of binary and ternary electrodeposits on AA7075 PDC. The optimized electrolyte bath parameters have been set so as to deposit uniform, less toxic, and environmentally friendly Zn-based binary and Ni-based ternary coatings on regular-shaped AA7075 PDC components.

Specimens of AA7075 PDC with high purity of size $20 \times 50 \times 2 \text{ mm}^3$ were made. These samples were mechanically smoothened with grit paper. Oil and grease were removed by a trichloroethylene agent. Acidic and alkaline cleaning were done followed by washing with distilled water and

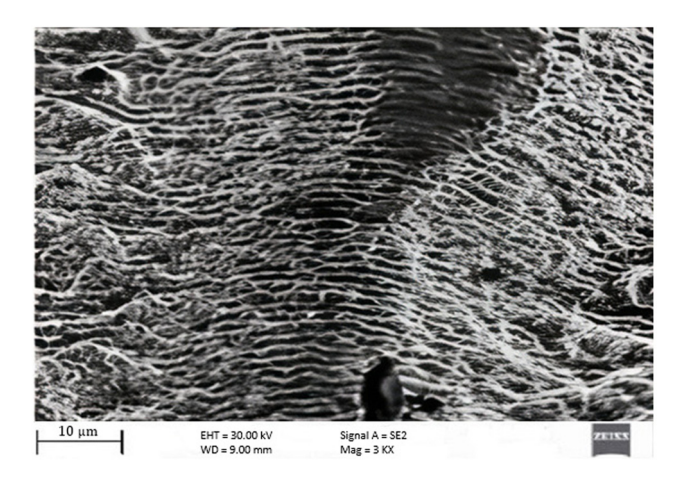


Figure 1: SEM image of LST surface.

Table 1: Optimized bath for Zn-Ni, Zn-Co, and Ni-Cr-Co coatings

Zn-Ni coating	Zn–Co coating	Ni–Cr–Co coating
NaOH = $96 \text{ g} \cdot \text{I}^{-1}$ (sodium hydroxide) ZnSO ₄ = $9 \text{ g} \cdot \text{I}^{-1}$ (zinc sulfate)	ZnSO ₄ ·6H ₂ O = 170 g·l ⁻¹ (zinc sulfate hexahydrate) CoSO ₄ ·6H ₂ O = 35 q·l ⁻¹ (cobaltous sulfate hexahydrate)	NiSO ₄ = 152 g·l ⁻¹ (sodium fluoride) NiCl ₂ = 29 g·l ⁻¹ (nickel(II) chloride)
NiSO ₄ = 3.45 g·l ⁻¹ (nickel(π) sulfate) NaF = 21 g·l ⁻¹ (sodium fluoride)	NaOH = 40 g·l ⁻¹ (sodium hydroxide)	$CrCl_3 = 122 \text{ g} \cdot l^{-1}$ (chromium chloride) $KHCO_2 = 8.5 \text{ g} \cdot l^{-1}$ (potassium formate)
pH = 11.6 Current density = 2 A·ft ⁻²	Boric acid = $18 \text{ g} \cdot \text{l}^{-1}$ (buffer) EDTA = $2 \text{ g} \cdot \text{l}^{-1}$	$NH_4Br = 19.5 \text{ g} \cdot \Gamma^{-1}$ (ammonium bromide) $KCl = 9.8 \text{ g} \cdot \Gamma^{-1}$ (potassium chloride)
Plating time = 17 min	(ethylene diamine tetraacetic acid)	Boric acid = $55.6 \text{ g} \cdot \text{l}^{-1}$
Observation: Uniform Zn-Ni deposition	Glycine = 8 g·l ⁻¹ (complexing agent)	$CoCl_2 = 78 \text{ g} \cdot \text{l}^{-1} \text{ (cobalt(II) chloride)}$ proprietary wetting agent = $0.16 \text{ g} \cdot \text{l}^{-1}$
	pH = 12.5 Current density = 9 A·ft ⁻²	Ammonium chloride = $28.5 \text{ g} \cdot \text{l}^{-1}$ pH = $2-3$
	Plating time = 20 min Observation: Uniform Zn–Co deposition	Current density = 500–520 A·ft ⁻² Plating time = 17 min Observation: Uniform Ni–Cr–Co deposition

then dried. The specimens' weight was noted using the digital weighing balance before and after the coating.

The optimized electrolyte baths were prepared for the binary and ternary electrodepositions and the parameters are given in Table 1.

The schematic of the electroplating arrangement for binary and ternary coatings on substrate material is displayed in Figure 2. The substrate material, *i.e.*, AA7075 PDC acted as a cathode (connected with the negative terminal) and coating materials such as Zn–Ni, Zn–Co, and Ni–Cr–Co are connected with the positive terminal (anode). The electrodes are immersed in the prepared electrolyte during the deposition. The optimized parameters were used for the binary and ternary coatings.

"Autosigma 3000 eddy current tester" has been used for checking the coating thickness at 500 kHz frequency.

The hardness and smoothness of surface coating increase the wear resistance. Microhardness is increased as the recrystallization of the coating occurs during the annealing process. It increases to a certain extent with an increase in annealing temperature to a certain extent, beyond which the hardness decreases. The optimum temperature for annealing is determined by the hardness test. In order to remove the residual stress in the uncoated and coated specimens, the specimens of size $2 \times 5 \times 0.2 \text{ cm}^3$ were annealed at 300°C for 8 h [6,13,16] and the hardness values were determined as per the ASTM-E-384 standard with 100 g load using Vickers' hardness testing equipment.

The abrasion resistance test was conducted as per the ASTM D-4060 standard on the coated alloy specimens of size $10 \times 10 \times 0.4$ cm³. The average weight loss was calculated by measuring the weight before and after the process.

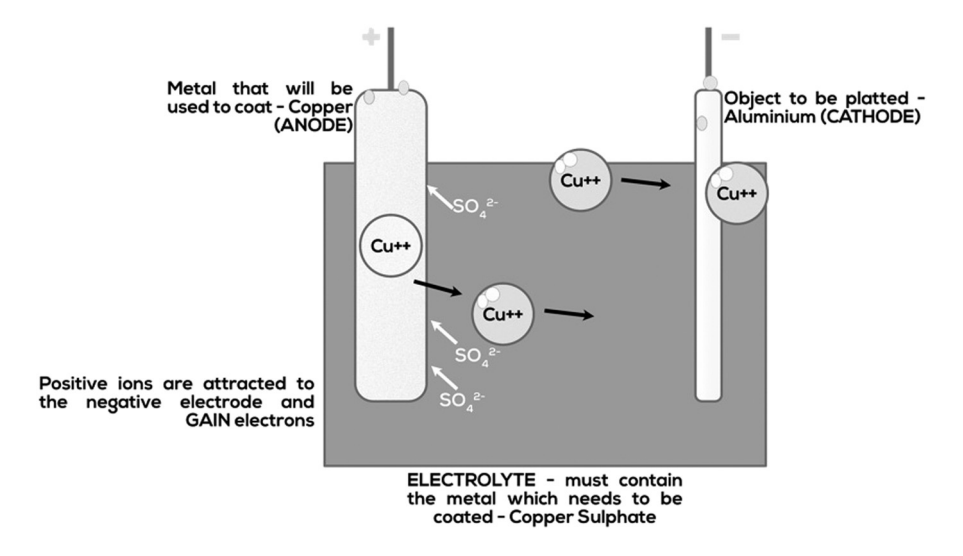


Figure 2: Schematic of electrodeposition arrangement.

A hard wheel with a load of 1,000 g was made to rotate for 1,000 cycles on the coated specimen.

Taber abrasion index = weight loss in 1,000 cycles.

A tensile test on the coated substrate was done according to the ASTM E8 standard to find out tensile strength. The tensile test was carried out using the Instron Universal Testing Machine with a strain rate of 2 mm·min⁻¹. A rectangular cross-section of samples was made and used as per the standard for the test. Vickers microhardness tester was used to find the hardness of uncoated and coated specimens. The coated and uncoated tensile specimens obtained after immersing them in Harrison's solution for a certain period have been used for conducting the tensile test. Harrison's solution is a mixture of 3.5% ammonium sulfate and 0.5% NaCl. The industrial environment has been simulated by this aqueous solution.

X-ray diffraction (XRD) patterns of alloy-coated PDC AA7075 specimens obtained from X' pert pro-XRD were analyzed to identify the intermetallic phases formed in the coatings. Cu $K\alpha$ radiation diffraction patterns of X-ray were obtained using 0.02° increment. The textured pattern was recorded by the X-ray technique with grazing incidents. Characteristics of coatings such as deposition nature, level of porosity, size of the grain, and heterogeneities present were studied using SEM. Samples of size $10 \times 10 \text{ mm}^2$ were used for SEM studies. SEM images were taken at 20,000 V with a magnification of $3,000 \times$.

To obtain the chemical composition of the coatings with the oxidation state of species, X-ray photoelectron spectroscopy (XPS) studies were carried out on alloy-coated AA7075 PDC samples of size $10 \times 10 \, \mathrm{mm}^2$ that were mounted in a chamber at 10^{-9} Torr. As per the ASTM B-117 standard, the corrosion studies were carried out on alloy-coated samples using SF 850 salt spray chamber. To simulate the effect of seawater, 3.5% NaCl was maintained inside the chamber. This type of aggressive environment starts corrosion on the coated surface. The degree of corrosion was recorded periodically and the appearance of red rust spots on samples in annealed condition was observed.

3 Results and discussion

3.1 Analysis of micro-hardness and Taber abrasion resistance on coated and uncoated materials

The microhardness of the binary and ternary coatings applied on the substrate material was measured and tabulated in Table 2.

Table 2: Microhardness measurements of coated and uncoated materials

S. No.	Deposition type	Microhardness (vickers hardness number) at 100 g load		
		As plated Heat-treated at 300°C		
1	Uncoated	115	243	
2	Zn-Ni	185	410	
3	Zn-Co	172	401	
4	Ni-Cr-Co	213	467	

Table 2 shows the microhardness of both binary and ternary coated and uncoated normal and annealed state of specimens. It is clearly evident from the table that the coated specimens have higher hardness than the uncoated specimens in both normal and heat-treated (annealed) state. Particularly, the ternary-coated specimen has higher hardness than the binary-coated specimen in both conditions [12].

For "non-heat-treated material," 50% of hardness enhancement is observed for the Zn–Co coating and 61% of improvement is observed for Zn–Ni coating compared to the uncoated condition. In the case of Zn–Ni binary coating, the increase in hardness could be due to the formation of fine grains with a meager porosity and the absence of microcracks [31]. The improved grain refinement could also be a reason for the hardness enhancement. The presence of smaller grains impedes the dislocation motion and increases microhardness. In the case of Zn–Co binary coating, the improvement in microhardness is the transformation of the whole Zn phase into a CoZn intermetallic one [10].

The ternary-coated specimen is observed to be higher (82%) among the coated specimens than the uncoated material. In the case of "heat-treated specimens," the minimum enhancement of hardness is observed as 65% for the Zn–Co alloy coating and a 69% improvement of hardness is observed for the Zn–Ni binary coating [32]. Similar to the non-heat-treated material, a higher hardness (92%) improvement is observed for ternary (Ni–Cr–Co) coating compared to the uncoated substrate material [33].

The presence of Cr as $\rm Cr_2O_3$ in Ni–Cr–Co coating with a binding energy of 576 eV at the outer layer in the ternary Ni–Cr–Co coating could be the reason for higher hardness than other binary depositions. Stress-relieving, recrystallization, and precipitation of deposited metals are the reasons for the increased hardness [22].

It is clearly evident from the analysis that the higher hardness enhancement is observed for the ternary coating compared to the uncoated and binary-coated specimens in both the status. Comparing the non-annealed and annealed materials, the uncoated specimen has more than double-fold enhancement in the hardness of the heat-treated material. A similar kind of hardness improvement is also observed for both the binary- and ternary-coated materials. It may be concluded that the heat-treated coated and uncoated specimens were found to have higher hardness than the non-annealed specimens due to relieving stress and affirmative alloy coating on the substrate material.

Microhardness results indicated that Ni–Cr–Co coatings showed higher hardness than the other two binary electrodeposited coatings. The following order of performance of coatings was observed from the microhardness studies: Ni–Cr–Co > Zn–Ni > Zn–Co.

The abrasion wear resistance of coated and uncoated materials of both the status such as heat treated and non-heat-treated specimens are provided in Table 3.

The Taber wear index value is an indicator of the wear resistance of the material. The lower the value, the higher will be the wear resistance. Based on the observation, the uncoated substrate material has lower abrasion resistance as it has a higher index value. The heat-treated uncoated specimen is also having a higher index value, which signifies the poor resistance to wear. In general, the coated specimens are exhibiting better wear resistance in both the heat-treated and non-heat-treated conditions. It has been observed from the table data that the ternary coating has

Table 3: Taber abrasion resistance measurement of coated and uncoated materials

S. No.	Deposition type	Taber wear index at load 1,000 g for 1,000 cycles		
		As plated	Heat treated at 300°C	
1	Uncoated	0.036	0.015	
2	Zn-Ni	0.014	0.007	
3	Zn-Co	0.022	0.012	
4	Ni-Cr-Co	0.013	0.005	

higher wear resistance than the binary-coated material. It has 64% higher resistance in the non-heat-treated status and 67% higher resistance in the heat-treated condition compared to the uncoated specimens. Among the binarycoated materials, Zn-Ni-coated material has higher wear resistance. It has 61% higher abrasion resistance compared to the uncoated specimen. On the other hand, it exhibits 53% higher wear resistance compared to the uncoated specimen in the case of heat-treated status. The annealed coated specimens still have better wear resistive properties compared to the non-annealed specimens. The wear resistance has been increased to almost two-fold in the heattreated specimens. The formation of NiZn₃ and Ni₂Zn₁₁ phase structure in the Zn-Ni deposits contributes to wear resistance. The submerging of Co particles in the galaxy of Zn atoms has led to improved wear resistance for the Zn-Co-coated material. The presence of Cr₂O₃ at the surface of Ni-Cr-Co coatings has improved the abrasion resistance in comparison with other electrodeposited coatings. The following order of performance of coatings was observed from the abrasion studies: Ni-Cr-Co > Zn-Ni > Zn-Co.

3.2 Analysis of tensile strength of coated and uncoated materials

The tensile test was conducted as per the ASTM E8 standard to evaluate the tensile strength of the binary and ternary deposition on the substrate materials. The mechanical strength studies have been undertaken after immersing the tensile specimens in Harrison's solution in order to simulate the industrial environment in real-time applications. The tensile specimen used for the present work is shown in Figure 3.

As demonstrated by the results of the tensile test, Ni–Cr–Co deposits exhibit excellent adhesion to AA7075 PDC substrates as depicted in Figure 4(a–c). In a similar

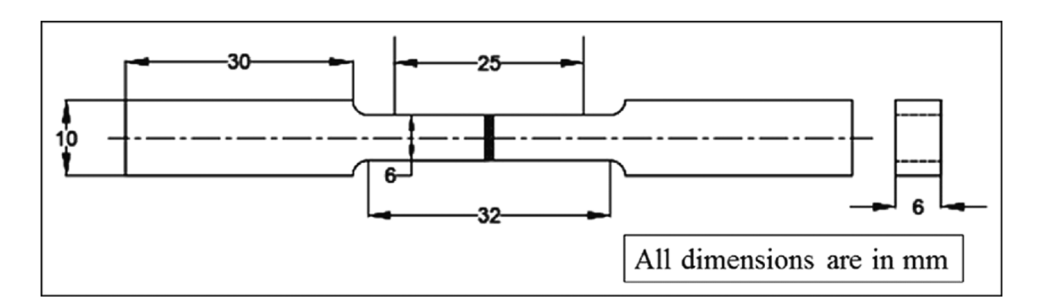


Figure 3: Tensile test sample as per ASTM E8 Standard.

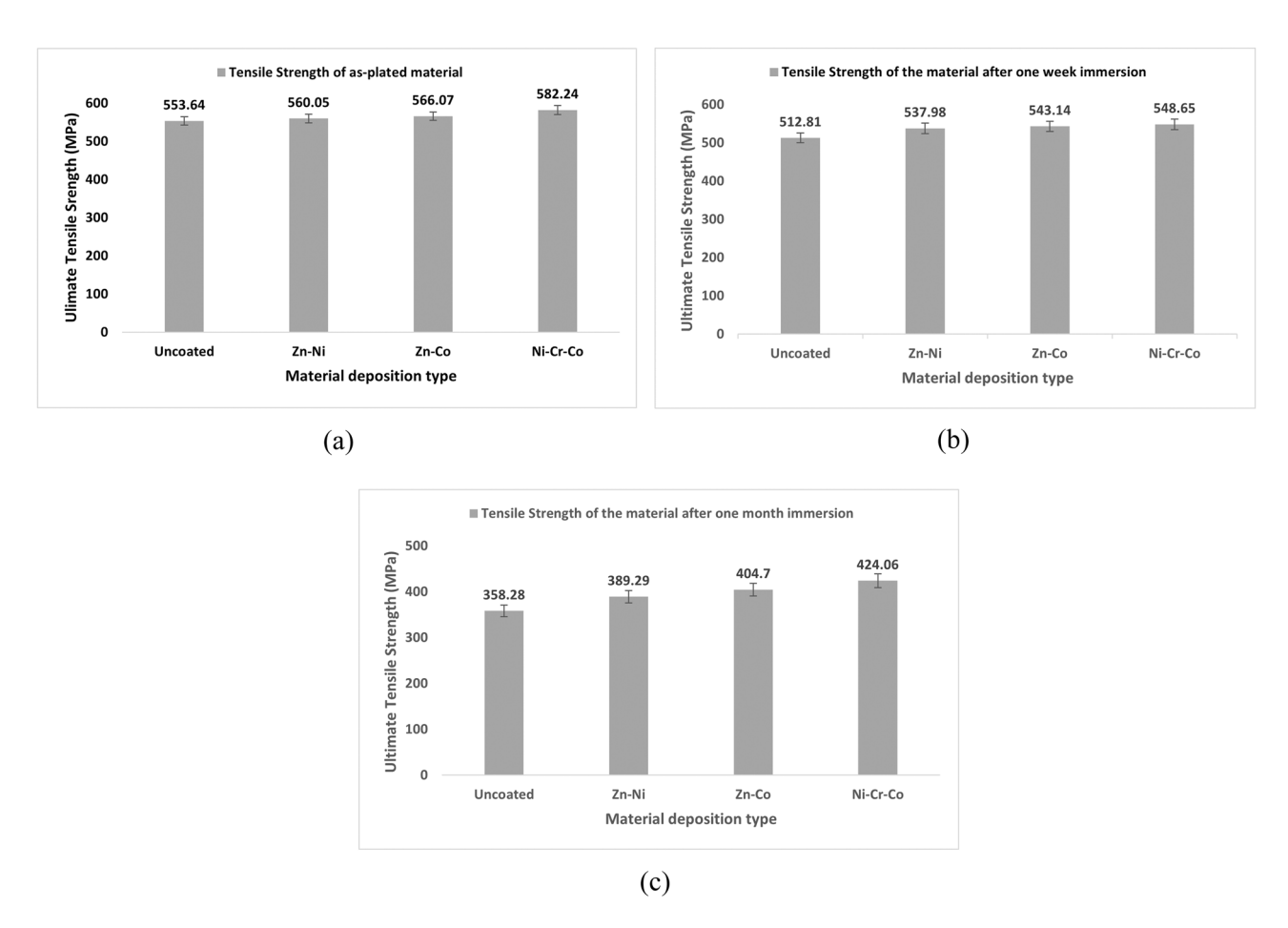


Figure 4: (a–c) Tensile strength of coated and uncoated deposited materials with and without immersion. (a) As-plated, (b) 1 week after immersion, and (c) 1 month after immersion.

fashion to the microhardness trend, the material that has been coated but has not been immersed has a higher tensile strength. However, for binary coatings, the enhancement percentage is in the range of 1 and 2. In comparison with the uncoated or substrate materials, ternary-coated materials have a maximum enhancement of 5% in tensile strength. In the case of deposits, there is an increase in tensile strength over uncoated deposits as a result of the cohesive strength of the coating, its load-bearing capacity, and the interlocking between the coating and anchoring points of the substrate. As a result of immersion in Harrison's solution for a week, the tensile properties of both coated and uncoated materials have deteriorated. For uncoated materials, the tensile strength has been reduced to a maximum of 7%, while for Zn-Ni binary-coated materials, the tensile strength has been reduced to a minimum of 3%. After immersion in the solution for a month, coated materials show a reduction in tensile strength of around 30%. After 1 week and 1 month of immersion, the uncoated material exhibits a higher reduction in tensile strength. The ternary-coated material, on the other hand, exhibits

a lesser reduction in tensile strength as compared to the substrate and binary-coated materials. In light of the test results, it seems that the ternary coating is capable of protecting the substrate to some extent regardless of the duration of the immersion.

Due to the presence of trimetallic atoms in Ni–Cr–Co, the surface coverage of this material has been enhanced to a greater degree. Furthermore, the chromium oxide layer has a better corrosion prevention characteristic, which may contribute to Harrison's solution's improved corrosion resistance as a result of the ternary electrodeposition.

The stress–strain curve for the uncoated AA7075 PDC substrate shows variations depending on the amount of stress applied and the resulting deformation as exhibited in Figure 5a. At low levels of stress, the material exhibits linear elastic deformation, which means that the deformation is reversible when the stress is removed. This is represented by the linear region on the stress–strain curve, known as the elastic region which indicates how stiff the material is. For uncoated AA7075, the modulus of elasticity is relatively high, indicating a stiff material. As the stress

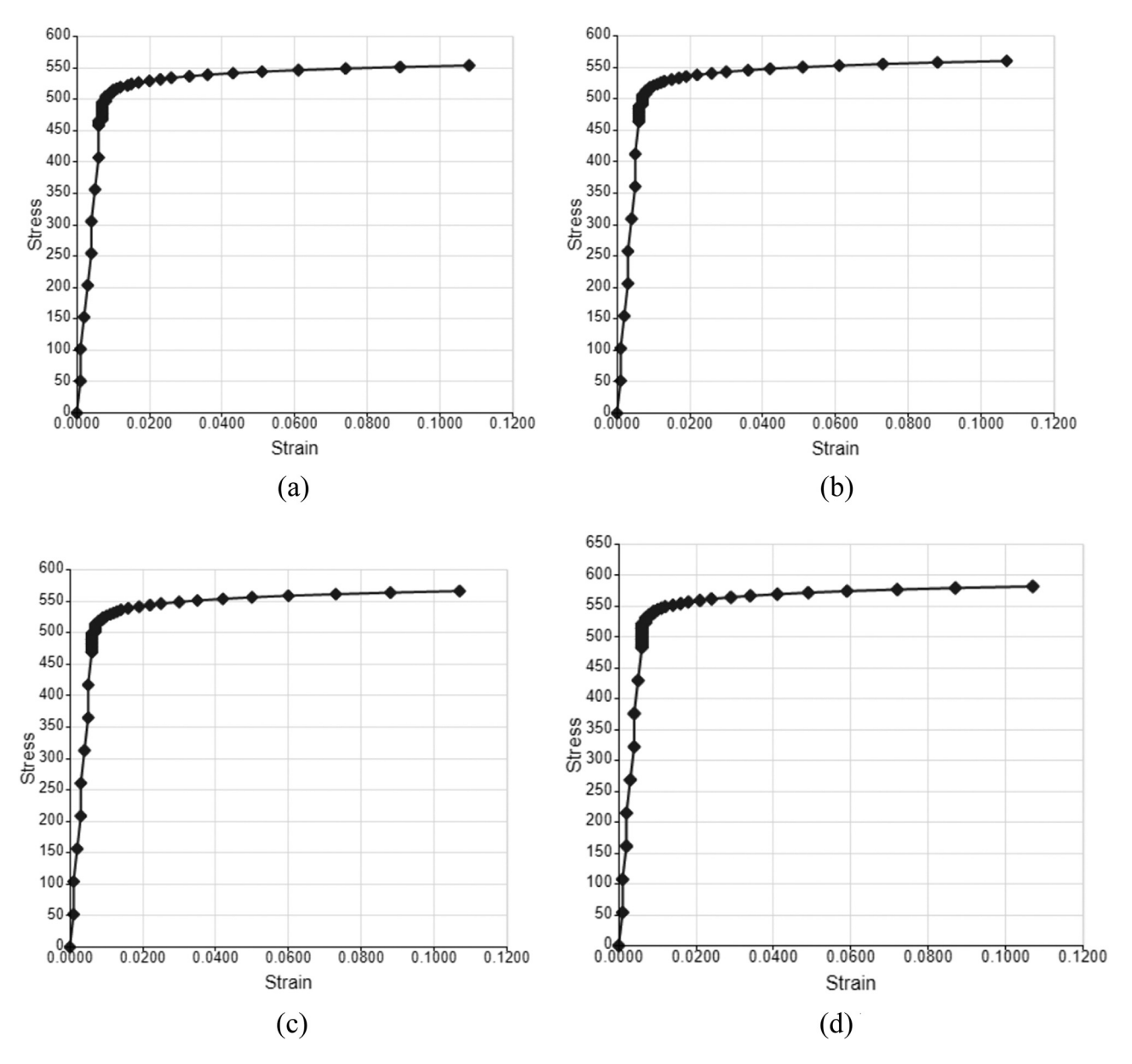


Figure 5: (a–d) Stress–strain curves of as-plated series. (a) Uncoated, (b) Zn–Ni deposited on AA7075 PDC, (c) Zn–Co deposited on AA7075 PDC, and (d) Ni–Cr–Co deposited on AA7075 PDC.

increases, the material begins to undergo plastic deformation, which is irreversible when the stress is removed. This is represented by the non-linear region on the stress—strain curve, known as the plastic region. The slope of this region decreases as the material undergoes more deformation, indicating that it becomes easier to deform as it approaches its ultimate tensile strength (UTS). At this point, the material undergoes necking, which is a localized reduction in cross-sectional area. The stress required to cause necking is referred to as the ultimate strength or tensile strength. The stress—strain curve for uncoated AA7075 also shows a region beyond the UTS, known as the post-necking region.

In this region, the material continues to deform until it eventually breaks. The slope of this region decreases as the material undergoes more deformation until it reaches its breaking point.

The mechanism of the stress-strain curve for uncoated AA7075 is related to the material's microstructure, which consists of a mixture of Al and Zn. As stress is applied, dislocations in the material's crystal structure move, allowing the material to deform. At low levels of stress, dislocations move only a small amount before returning to their original position, resulting in elastic deformation. As the stress increases, dislocations move further, resulting in plastic

deformation. In summary, the stress–strain curve for the uncoated AA7075 PDC substrate shows variations in its response to external stress, which can be attributed to the material's microstructure. The curve exhibits a linear elastic region, a non-linear plastic region, a necking region, and a post-necking region, culminating in eventual failure as exhibited in Figure 5a.

Zn–Ni coatings deposited on the AA7075 substrate improve the material's corrosion resistance, wear resistance, and adhesion. The stress–strain curve for Zn–Nicoated AA7075 shows an increase in the UTS and a smoother transition from elastic to plastic deformation, compared to uncoated AA7075 as exhibited in Figure 5b. The coating prevents the formation of microcracks and distributes stress more evenly, leading to an increase in UTS and improved mechanical strength.

Zn–Co coatings deposited on AA7075 improve corrosion resistance, wear resistance, and adhesion. The stress–strain curve for Zn–Co-coated AA7075 shows an increase in UTS and a slightly steeper slope in the elastic region compared to uncoated AA7075 as exhibited in Figure 5c. The coating's enhanced adhesion to the substrate improves the mechanical strength of the material, leading to an increase in UTS as exhibited in Figure 5c.

Ni–Cr–Co coatings deposited on AA7075 improve wear resistance, adhesion, and high-temperature stability. The stress–strain curve for Ni–Cr–Co-coated AA7075 shows a slight increase in UTS and a steeper slope in the elastic region compared to uncoated AA7075 as exhibited in Figure 5d. The coating's ability to reduce friction and prevent wear leads to an improvement in the material's mechanical strength.

Overall, each coating has a unique impact on the mechanical properties of AA7075, as seen from the stress–strain curves. Zn–Ni and Zn–Co coatings improve corrosion resistance, wear resistance, and adhesion, leading to an increase in UTS and improved mechanical strength. Ni–Cr–Co coatings improve wear resistance, adhesion, and high-temperature stability, resulting in a slight improvement in UTS and mechanical strength.

The tensile test was conducted on the uncoated and coated specimens after immersing them in Harrison's solution for a period of 1 week and 1 month. The results of the tests are provided in Table 4.

It has been observed that the appearance of the fracture planes existed within the deposit, which signifies the cohesive type of fracture. In all the cases, the fracture is found nearer to the interface between the deposit and the substrate, but still inside the deposit. No external peeled-off layer is noticed. Ni–Cr–Co deposit has remarkable adhesion on AA7075 PDC substrates, showing good bonding

Table 4: Tensile test results of coated and uncoated materials immersed in Harrison's solution

S. No.	Deposition	UTS (MPa)			
	type	As plated	1 week after immersion	1 month after immersion	
1.	Uncoated	553.64	512.81	358.28	
2.	Zn-Ni	560.05	537.98	389.29	
3.	Zn-Co	566.07	543.14	404.70	
4.	Ni-Cr-Co	582.24	548.65	424.06	

between the deposit and substrate, evidenced by the result of the tensile test.

Similar to the microhardness trend, the tensile strength is also higher for the coated non-immersed materials. However, the percentage enhancement is in the order of 1 and 2 for the binary coatings. The ternary-coated material has a maximum of 5% enhancement in the tensile strength compared to the uncoated material or substrate material. The reasons for the increase in tensile strength of deposit over uncoated material are due to the cohesive strength of the surface deposit, its load-bearing capacity, and the interlocking of deposit with anchoring points of the substrate, which is made by LST.

The tensile property of both the coated and uncoated materials has deteriorated while they are immersed in Harrison's solution for a week. The tensile strength has been reduced to a maximum extent of 7% for uncoated material and a minimum (3%) for Zn–Ni binary-coated material.

The percentage reduction in tensile strength is found to be around 30% in the case of coated materials after they are immersed in the solution for a month. The uncoated material is found to have a higher reduction in tensile strength for the 1-week and 1-month immersion periods. On the other hand, the ternary-coated material has a lesser reduction in tensile strength compared to the substrate and binary-coated materials. It is understood from the test results that the ternary coating protects the substrate to some extent irrespective of the immersion periods.

The presence of tri-metallic atoms in Ni–Cr–Co has enhanced the surface coverage to a larger extent. Also, the chromium oxide layer possesses a better corrosion prevention characteristic and these aspects could be the reasons for ternary electrodeposition enriching the performance against the corrosion in Harrison's solution.

It is demonstrated that the tensile strength (MPa) of Ni–Cr–Co on AA7075 PDC is higher than the other deposits (582.24 of Ni–Cr–Co > 566.07 of Zn–Co > 560.05 of Zn–Ni > 553.64 of uncoated condition) due to the existence of hard

Cr particles along with its strong bonding between the intermetallic atoms such as Ni and Co [32].

Further, it is observed that the presence of crystal orientation (XRD studies), phase content (XPS studies), and surface morphology of ternary Ni–Cr–Co have greatly contributed to the enhancement of tensile strength. The following order of performance of coatings is observed from the tensile test: Ni–Cr–Co > Zn–Co > Zn–Ni [33].

3.3 XRD and SEM image analysis of coated materials

The XRD pattern of both the binary- and ternary-coated materials is depicted in Figure 6(a–c).

The XRD analysis of the Zn–Ni binary coating is shown in Figure 6(a). The diffraction peaks of γ -NiZn₃ (831), γ -Ni₂Zn₁₁ (330), and 631 with 2 θ values 38, 43, and 73° are confirming the presence of Zn–Ni binary deposit on AA7075 PDC substrate. A further peak of about 56, 68, and 83° is indicative of Zn deposits in the Zn–Ni coatings (102, 110, and 200). The coatings have enhanced hardness value due to the presence of intermetallic phases.

The XRD pattern of Zn–Co-coated material is depicted in Figure 6(b). The presence of three strong peaks such as Zn (110), Co (111), and CoZn (211) and two feeble peaks such as ϵ -CoZn₃ (220) and ϵ -CoZn₃ (301) is clearly visible. Besides, there is a very weak peak at 61.8° for α -Al (112) proving that Zn–Co coatings have been carried out on AA7075 PDC substrate.

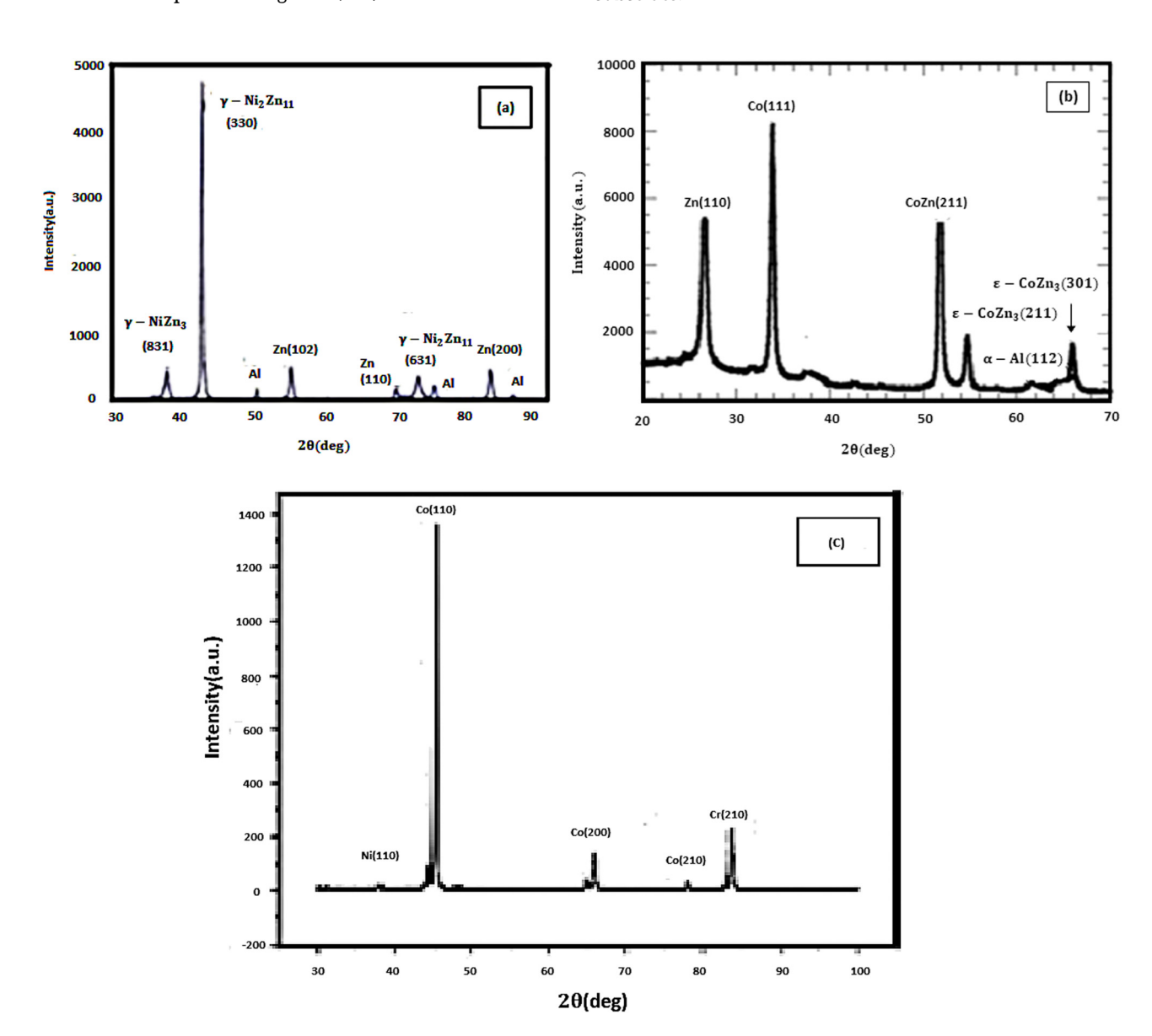
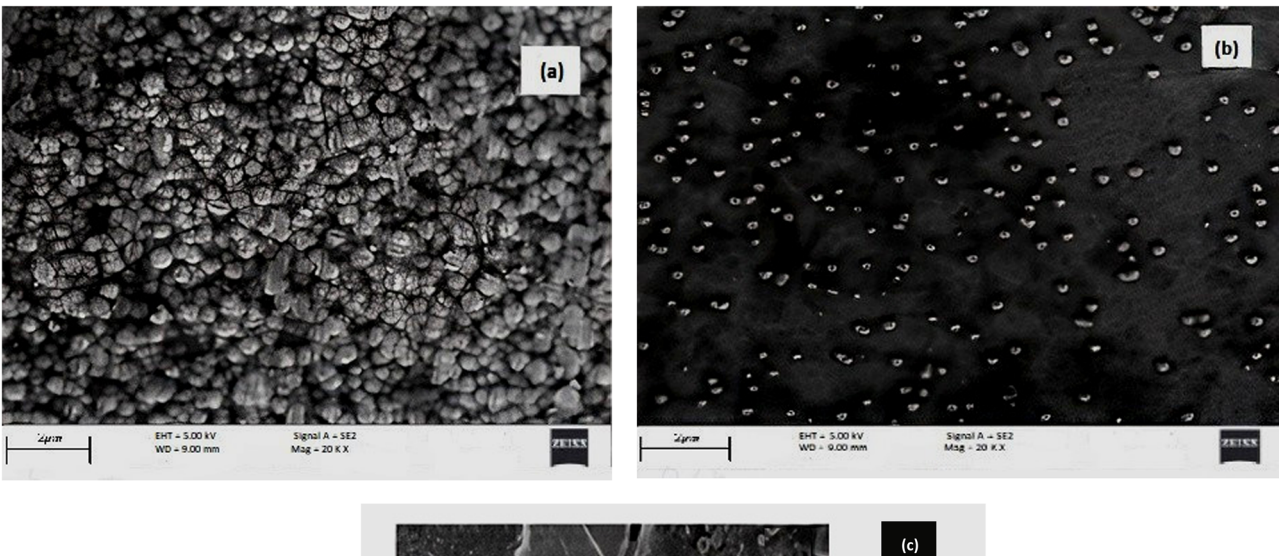


Figure 6: (a-c) XRD patterns of (a) Zn-Ni (b) Zn-Co and (c) Ni-Cr-Co-coated materials.

The XRD pattern of Ni–Cr–Co ternary coating is displayed in Figure 6(c). It can be seen from the pattern that the Ni–Cr–Co ternary deposit is a solid solution with a body-centered cubic structure due to the formation peaks at lattice plane such as (110), (220), and (210) with a crystal lattice constant of 2.88 A°. Among them, the Co phase has clear, sharp diffraction peaks at θ of near 45.168, 65.792, and 77.392°, and their crystal plane index is (110), (200), and (210), respectively. The peaks in XRD are sharp, narrow, and regular and therefore, all the coatings Zn–Ni, Zn–Co, and Ni–Cr–Co are crystalline. The intensity of the peak is in accordance with the JCPDS card number 03-074-1264.

The SEM image has been taken on both the binary- and ternary-coated materials and is shown in Figure 7(a–c).

The deposited surface displays many shallow pits due to hitting by progressive particles. The deficient and twisted particles are observed in the image. The uniformity in deposition attributes to a conservative structure, low porosity, and high deposition of coatings. The SEM image illustrated in Figure 7(a) shows the presence of smaller globular structure Zn-Ni atoms. Moreover, the atoms are overcrowded owing to the strong bonding between Zn and Ni and further effective adhesion of said coatings on LST AA7075 substrate. The uniformly dispersed Zn-Ni particles in the deposition are also observed. The surface morphology of binary Zn-Co coating on the PDC AA7075 substrate is shown in Figure 7(b). The evenly distributed dot-like structure and submerged Co particles in the galaxy of Zn atoms have been observed in the image. Further, it has been demonstrated that the incorporation of Co atoms in the Zn matrix is highly visible. To remove the oxide film on the AA7075 PDC, the zincating process was carried out. The deposition of Zn on the surface of Al created a suitable site for Zn nucleation. Since it is a chemical immersion coating, the aggressive nature of sodium hydroxide present in the zincating bath had thrown Zn atoms on AA7075 PDC, leading to a more uniform distribution of Zn atoms.



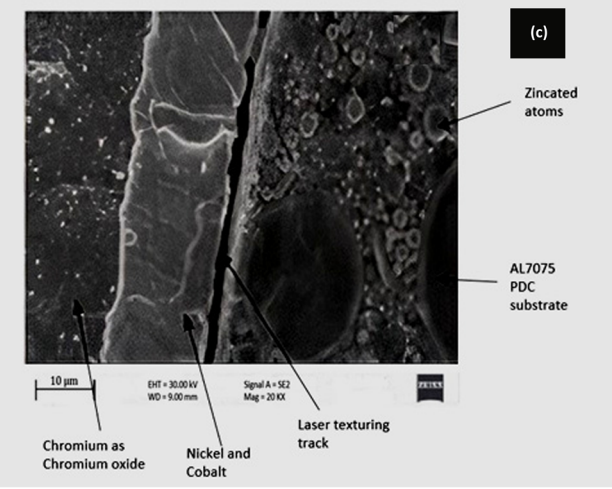


Figure 7: (a-c) SEM image of the (a) Zn-Ni (b) Zn-Co and (c) Ni-Cr-Co-coated materials.

Good differentiation was achieved in the area between the laser track among the Ni-Cr-Co coatings and Al layers. The coverage of laser track and Ni-Cr-Co coatings is very obvious, confirming the better diffusion of Ni-Cr-Co coatings than Zn-Co-coated AA7075 PDC substrate. To understand the effectiveness of bonding by laser texturing, cross-section SEM has been carried out and shown in Figure 7(c). It is understood from the image that the effective adhesion of Ni-Cr-Co on AA7075 PDC had taken place and the same could also be the reason for the enhancement of microhardness, wear, and corrosion resistance of the said coating. The image shown in the SEM contained three parts: a) the substrate AA7075, b) the track of laser texturing, and c) the oxides of Ni-Cr-Co. It is established that the formation of unique and uniform oxide depositions on the top layer of Ni-Cr-Co has significantly contributed to higher retardation of metal attack on Ni-Cr-Co in the corrosive medium.

3.4 Analysis of XPS on binary- and ternarycoated materials

The analysis of XPS on binary- and ternary-coated materials has been carried out and the results are shown in Table 5 and Figure 8.

The results of XPS studies on the binary- and ternarycoated materials are provided in Table 5. It provides information about the species formed, binding energy, electron level, and the type of layer on XPS investigation of coated materials. Figure 8(a) shows the XPS analysis of the Zn-Ni deposit on AA7075 PDC. Two major Ni peaks in the highresolution XPS arose from 2p signals located around 856 and 874 eV, which were the characteristics of 2p3 = 2 and 2p1 = 2, respectively. Moreover, there are two peaks referred to as satellite peaks around 2p3 = 2 (S) and 2p1 = 2 (3S) in the Ni 2p region. Remarkably, the presence of Ni₂Zn₁₁ demonstrated lower binding energy in comparison with -NiZn₃.

The results of XPS of Zn-Co on the AA7075 PDC substrate are shown in Figure 8(b). The existence of Co as Co₃O₄ in the inner layer of the coating is confirmed by O KLL with a binding energy of 1,008 eV, which has proximity to peaks of $Co_2p_3 = 2$ with the binding energy of 779 eV. It is justified that the Co could have existed as Co₃O4 in the coating. The binding energies resulting at 1,074, 853, and 839 eV are attributed to the presence of Zn metal in the coating. Further, the appearance of O KLL at 1,008 eV might be due to the formation of ZnO in the coating. It is peculiar to note that there is a sharing of oxygen atoms between Zn and Co metals which appeared as Zn and Co₃O₄ in the coating.

The XPS analysis on ternary-coated material is displayed in Figure 8(c). The XPS output shows the existence of Cr, Co, and Ni alloy composition on the surfaces of coatings. Adventitious C and N peaks have entered the laboratory atmosphere. The complex peaks of Co 2p, Ni 2p, and Cr 2p exhibit binding energies that correlated with the presence of Co₃Zn₃, NiO, and CrO₃, respectively. The sub-peaks in Zn 2p and Al 2p 1s peak revealed the zincating of the substrate material.

3.5 Analysis of salt spray on uncoated and coated materials

A salt spray test has been conducted on the substrate and the heat-treated-coated specimens. To analyze the corrosion resistance of materials, changes in appearance due to prolonged periods of exposure to a corrosive environment are considered. The results of the salt spray test on specimens are provided in Table 6.

The appearance and progress of corrosion of uncoated and Zn-Ni-coated samples under salt spray were recorded from time to time. After 60 min stay, it was noticed that 40% rust formed on uncoated AA7075. For the heat-treated

Table 5: XPS	of b	inary- a	and t	ernary	-coated	materials
--------------	------	----------	-------	--------	---------	-----------

SI. No.	Material deposition	Species identified	Binding energy (eV)	Electron level	Layer
1	Zn-Ni (binary)	y-NiZn₃	856, 874	2p3/2, 2p	Inner layer
		y-Ni ₂ Zn ₁₁	631	LMM	Outer layer
2	Zn-Co (binary)	Cobalt as Co ₃ O ₄	779	2p3/2	Outer layer
		O KLL	1,008	_	Inner layer
		Zinc as ZnO	1,074, 853 and 839	2p	Inner layer
3	Ni-Cr-Co (ternary)	Co	884	2p	Inner layer
		NiO	689	1s, 3p, and LMM [quantum state]	Inner layer
		Cr as Cr ₂ O ₃	576	2p	Outer layer

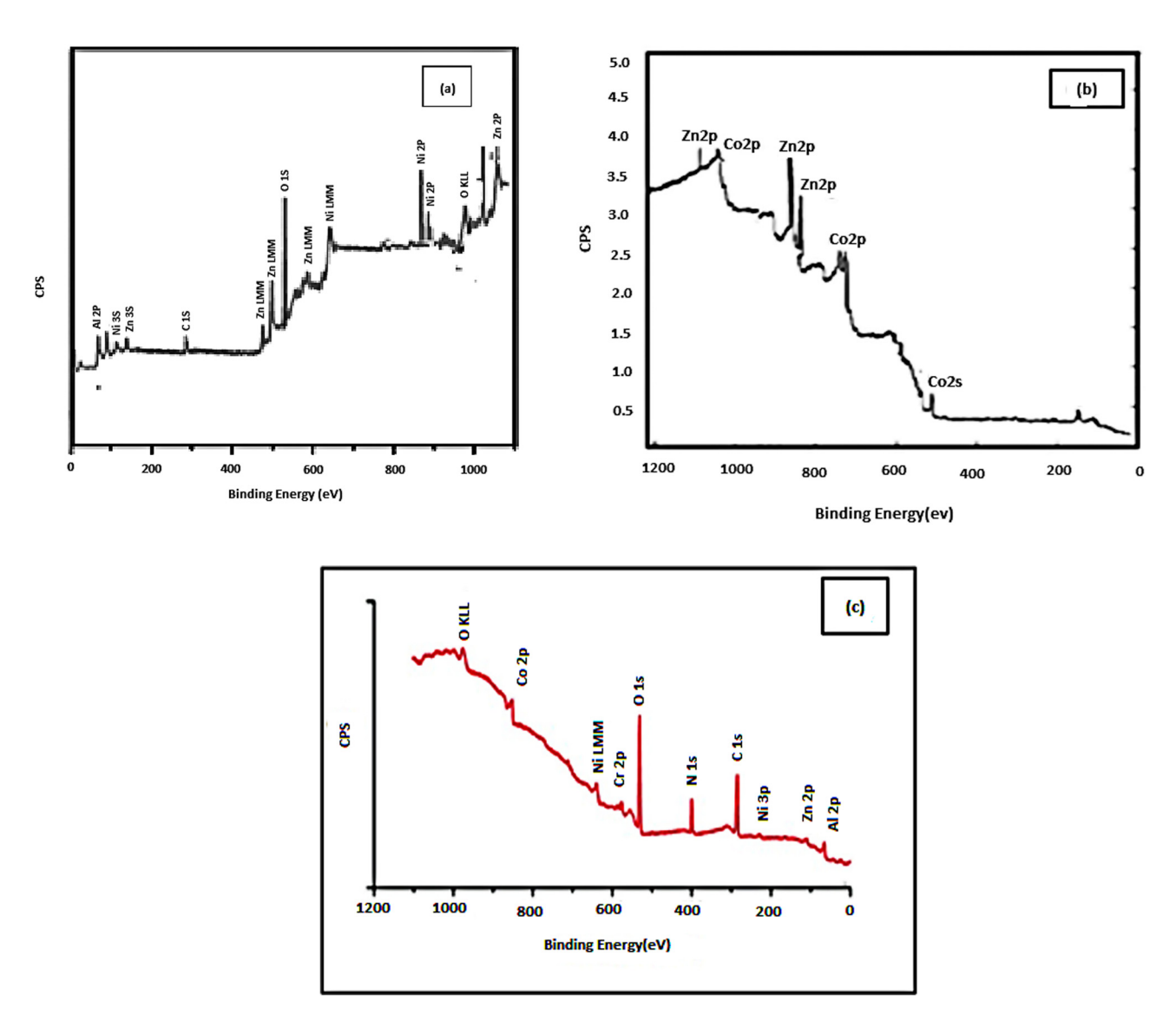


Figure 8: (a-c) XPS of coated materials (a) Zn-Ni, (b) Zn-Co, and (c) Ni-Cr-Co.

sample, 1% rust area was formed after 610 h of stay in the salt spray chamber. Zn–Ni nano-crystalline coating could be obtained with higher current efficiency on a single Y phase. This Y phase shows the highest corrosion protection. The XRD analysis of Zn–Ni shows the Y phase of intermetallic NiZn₃, and Ni₂Zn₁₁ retards the corrosion formation. The homogeneity in phase composition leads to the upgradation of corrosion protection properties. With various Ni content, the internal stress of deposit was found by the X-ray stress analyzer and concluded that a sudden increase in salt spray time was due to the penetration of corrosion products as a result of a shoot up in internal stress. The selective corrosion of the Zn–Ni deposit occurs in the following sequence deposit: a) dissolving of Zn, b) passivation, and c) crack propagation. Hence, it is understood that the

enhancement of corrosion resistance for coated surfaces might be due to the formation of $-NiZn_3$ and $-Ni_2Zn_{11}$ [12].

It is observed from the table that the heat-treated Zn–Co electrodeposition on AA PDC 7075 has shown 1% of rust area formed after 550 h of stay in the salt spray chamber. The application of a reverse pulse current to suppress the zinc hydroxide formed the maximum percentage of Co in the coatings [38,39]. The controlled morphology and the composition of binary Zn–Co deposits minimize the internal stress and micro-cracks. The formation of refined grains of Co atoms is uniformly dispersed in the Zn matrix in the coatings. The reason for corrosion resistance improvement of binary Zn–Co deposits could be because the binary Zn–Co deposits consist of fine globular Co particles submerged in the galaxy of Zn atoms as ZnO shown in the SEM image.

Table 6: Results of salt spray test on uncoated and coated materials

Time (h)	Surface appearance of AA7075 PDC samples						
	Uncoated	Zn–Ni deposited	Zn-Co deposited	Ni-Cr-Co deposited			
0	Nil	Bright	Bright	Bright			
1	40% rust area	Semi dull	Semi dull	Semi dull			
42	Fully corroded	Semi dull	Semi dull				
50	Fully corroded			Semi dull			
100	Fully corroded			Semi dull			
120	Fully corroded	Semi dull	Semi dull				
150	Fully corroded			Semi dull			
200	Fully corroded			Dull			
240	Fully corroded	Semi dull	Semi dull				
480	Fully corroded	Dull	Dull				
550	Fully corroded		1%				
			rust area				
610	Fully corroded	1% rust area	7%				
			rust area				
650	Fully corroded						
660	Fully corroded			1%			
				rust area			
700	Fully corroded	7% rust area					
750	Fully corroded			7%			
	-			rust area			
1,100	Fully corroded		50%				
			rust area				
1,200	Fully corroded	50%					
	-	rust area					
1,300	Fully corroded			50%			
	-			rust area			

The analysis of salt sprays on ternary Ni–Cr–Co electrodeposition on AA7075 PDC is also provided in the table. The presence of trivalent Cr as an oxide in the phase of Cr as $\rm Cr_2O_3$ at the outer layer has a binding energy of 576 eV in the ternary coating. Further, the maximum content of Zn (94.8%) with Co (5.2%) has led to 1% rust formation with a delayed time (660 h).

Compared with the binary deposit Zn–Ni and Zn–Co, the ternary Ni–Cr–Co deposit is found to have more Ni and Co concentration, as higher current density (500–550 A·ft⁻²) followed [40–42]. The reason for higher Ni and Co content in the ternary coating is the synergistic catalytic effect in the electrolyte bath [43–45]. The presence of a crystalline structure with the high alignment of Co and Ni atoms could significantly improve the corrosion resistance of Ni–Cr–Co coatings on AA 7075 PDC substrates [46–48]. In addition, the formation of the passive oxide layer on Cr has justified its corrosion resistance performance in the rankings [49–51]. All in all, the Al alloy AA7075 is broadly used in various industries owing to its high strength-to-weight ratio, which is comparable and replaceable to steel in many applications [52–54].

However, it has poor resistance to wear and corrosion compared to other Al alloys. To improve the mechanical, wear, and corrosion properties of AA7075, a novel coating method has been developed. Binary and ternary metals such as Zn-Ni, Zn-Co, and Ni-Cr-Co are electroplated on the substrate material (AA7075) after LST pre-treatment. According to the ternary coating results, the resistance of the specimens under non-heat-treated conditions is higher than the resistance of specimens under heat-treated conditions [55–57]. The Ni-Cr-Co ternary coating has higher tensile strength compared to other deposits [58–60]. The SEM images, XRD, and XPS findings on the coated materials have been corroborated with the analyses on mechanical and corrosion properties. The dendritic structure during solidification leads to deterioration in the mechanical properties of AA7075 PDC [61–63]. To improve the performance in automotive and aircraft applications, the present research work is focused to develop novel electrodeposition of binary and ternary coatings by LST on AA7075 PDC material for the enhancement of hardness, tensile strength, wear, and corrosion resistance of substrate material to lengthen the life span of AA7075 in actual applications [64-66]. The optimized parameters have been used for the surface coatings on AA7075 PDC in the present study [67–69]. Electrodeposited coatings of Zn–Ni, Zn-Co, and Ni-Cr-Co have become increasingly popular in recent years due to their unique properties and various applications [70-72]. Here are some of the applications of these novel coatings on AA7075.

- Corrosion protection: Electrodeposited Zn–Ni, Zn–Co, and Ni–Cr–Co coatings have excellent corrosion resistance properties. These coatings can protect the underlying AA7075 from corrosion in various environments such as seawater, acidic and alkaline solutions, and humid and corrosive atmospheres [73–75].
- 2) Wear resistance: These coatings also exhibit high wear resistance, which is useful in applications that involve sliding, rolling, or abrasive wear. For instance, these coatings can be applied to components in the automotive, aerospace, and marine industries to enhance their wear resistance [76,77].
- 3) Thermal stability: Electrodeposited coatings of Zn–Ni, Zn–Co, and Ni–Cr–Co are also known for their high thermal stability. This property makes them suitable for use in high-temperature applications where other coatings may fail. For example, these coatings can be used on heat exchangers and other components that are exposed to high temperatures [78,79].
- 4) Decorative finishes: These coatings can also be used for decorative purposes due to their attractive appearance. The Zn-Ni, Zn-Co, and Ni-Cr-Co coatings can be easily

plated onto AA7075 to provide a durable and aesthetically pleasing finish [80,81].

In summary, electrodeposited Zn–Ni, Zn–Co, and Ni–Cr–Co-based coatings have various applications on AA7075, including corrosion protection, wear resistance, thermal stability, decorative finishes, electrical conductivity, and biomedical applications. Hence, the order of corrosion resistance performances of the coating in 3.5% NaCl is as follows: Ni–Cr–Co > Zn–Ni > Zn–Co.

4 Conclusions

A comprehensive experimental investigation has been carried out on a novel electrodeposited coating on LST AA7075 PDC to improve the mechanical, abrasion, and corrosion resistance properties for the application of automobile and aviation structure components. A new bath formulation based on binary and ternary coatings as an alternate to the cadmium electroplating process has been developed and found stable throughout the various experimental conditions. All these coatings on the AA7075 PDC substrate improve the mechanical properties and corrosion resistance to a greater extent. The highlighted result outcomes are provided as follows:

- The optimized plating parameters have been used for the deposition of binary and ternary electrodeposits on AA7075 PDC.
- 2) The coated materials have higher hardness than the uncoated material. Particularly, the ternary (Ni–Cr–Co) coating is found to have higher hardness than the binary electrodeposited coatings due to the formation of $\rm Cr_2O_3$ phases in the coating.
- 3) The heat-treated-coated materials have a higher scale of enhancement in microhardness.
- 4) Based on the hardness studies, the materials can be rated as Ni–Cr–Co > Zn–Ni > Zn–Co > uncoated.
- 5) Similar to microhardness, the presence of Cr₂O₃ at the surface of Ni–Cr–Co coating has improved the abrasion resistance when compared to the binary electrodeposited coatings.
- 6) The tensile strength (MPa) of Ni–Cr–Co on AA7075 PDC is more than all other deposits (582.24 of Ni–Cr–Co > 566.07 of Zn–Co > 560.05 of Zn–Ni > 553.64 of uncoated condition) due to the existence of hard Cr particles along with its strong bonding with intermetallic atoms such as Ni and Co.
- 7) The salt spray analysis indicated that all the coatings exhibited better corrosion resistance. The high corrosion

- resistance value is observed for ternary coating and followed by Zn–Ni and Zn–Co binary coatings.
- 8) There is no agglomeration observed in plating formation. The impressive performances of the electrodeposited coatings could be attributed to the presence of intermetallic phases, the uniform arrangement of atoms, augmented ductility, and high dispersion of metallic particles on the surface of coatings, which are evidenced by the SEM and XPS studies.
- 9) From binding energy values (576 eV) for Ni–Cr–Co coatings, the outer layer consisted of Cr as Cr_2O_3 which is highly harder than the other coatings, which could be the reason for its fabulous performance in comparison with all other coatings.
- 10) Based on the XRD analysis, the formation of intermetallic phases in the coated material could have contributed to their improved mechanical properties in comparison with uncoated AA7075 PDC.

At the outset, the electrodeposited Ni–Cr–Co coatings are recommended for aircraft and automobile parts due to the impressive performances of the said coatings. The performances of Zn–Ni in enhancing the mechanical properties of AA7075 PDC have justified its position in the rankings.

Funding information: The authors state no funding involved.

Author contributions: All authors have accepted responsibility for the entire content of this manuscript and approved its submission.

Conflict of interest: The authors state no conflict of interest.

References

- [1] Williams, J. C. and E. A. Starke, Jr. Progress in structural materials for aerospace systems. *Acta Materialia*, Vol. 51, No. 19, 2003, pp. 5775–5799.
- [2] Kermanidis, A. T. Aircraft aluminum alloys: applications and future trends. In *Revolutionizing Aircraft Materials and Processes*, Springer, Cham, 2020, pp. 21–55.
- [3] Campbell Jr F. C. Manufacturing technology for aerospace structural materials, Elsevier, 2011.
- [4] Meng, Q. and G. S. Frankel. Effect of Cu content on corrosion behavior of 7xxx series aluminum alloys. *Journal of the Electrochemical Society*, Vol. 151, No. 5, 2004, id. B271.
- [5] Pattnaik, S., D. B. Karunakar, and P. K. Jha. Developments in investment casting process – A review. *Journal of Materials Processing Technology*, Vol. 212, No. 11, 2012, pp. 2332–2348.

- [6] Niu, X., B. Hu, I. Pinwill, and H. Li. Vacuum-assisted high pressure die casting of aluminum alloys. *Journal of Materials Processing Technology*, Vol. 105, 2000, pp. 119–127.
- [7] Dahle, A. K., Y. C. Lee, M. D. Nave, P. L. Schaffer, and D. H. StJohn. Development of the as-cast microstructure in magnesium-aluminum alloys. *Journal of light metals*, Vol. 1, No. 1, 2001 Feb 1, pp. 61–72.
- [8] Blondheim, D. and A. Monroe. Macro porosity formation: a study in high pressure die casting. *International Journal of Metalcasting*, Vol. 16, No. 1, 2022 Jan, pp. 330–341.
- [9] Brito, V. S., I. N. Bastos, and H. R. Costa. Corrosion resistance and characterization of metallic coatings deposited by thermal spray on carbon steel. *Materials & Design*, Vol. 41, 2012 Oct 1, pp. 282–288.
- [10] Hillier, E. M. and M. J. Robinson. Hydrogen embrittlement of highstrength steel electroplated with zinc-cobalt alloys. *Corrosion Science*, Vol. 46, No. 3, 2004 Mar 1, pp. 715–27.
- [11] Sriraman, K. R., S. Brahimi, J. A. Szpunar, and S. Yue. Hydrogen embrittlement of Zn-, Zn-Ni, and Cd-coated high strength steel. *Journal of Applied Electrochemistry*, Vol. 43, No. 4, 2013 Apr, pp. 441–451.
- [12] Yang, Y. F., Z. Q. Gong, L. Y. Deng, B. P. Luo, Y. T. Ma, and Z. H. Yang. Electrodeposition of Ni-Cr alloy on an aluminum substrate. *Journal of the Central South University of Technology*, Vol. 13, No. 3, 2006 Jun, pp. 219–224.
- [13] Pushpavanam, M., H. Manikandan, and K. Ramanathan. Preparation and characterization of nickel–cobalt-diamond electro-composites by sediment co-deposition. *Surface and Coatings Technology*, Vol. 201, No. 14, 2007 Apr 2, pp. 6372–6379.
- [14] Lee, W. H., S. C. Tang, and K. C. Chung. Effects of direct current and pulse-plating on the co-deposition of nickel and nanometer diamond powder. *Surface and Coatings Technology*, Vol. 120, 1999 Nov 1, pp. 607–611.
- [15] Ghanbari, S. and F. Mahboubi. Corrosion resistance of electrodeposited Ni-Al composite coatings on the aluminum substrate. *Materials & Design*, Vol. 32, No. 4, 2011 Apr 1, pp. 1859–1864.
- [16] Ozga, P. and E. Bielańska. Determination of the corrosion rate of Zn and Zn–Ni layers by the EDS technique. *Materials Chemistry and Physics*, Vol. 81, No. 2–3, 2003 Aug 28, pp. 562–565.
- [17] Byk, T. V., T. V. Gaevskaya, and L. S. Tsybulskaya. Effect of electrodeposition conditions on the composition, microstructure, and corrosion resistance of Zn–Ni alloy coatings. *Surface and coatings technology*, Vol. 202, No. 24, 2008 Aug 15, pp. 5817–5823.
- [18] Deqing, W., S. Ziyuan, and K. Tangshan. Composite plating of hard chromium on the aluminum substrate. *Surface and Coatings Technology*, Vol. 191, No. 2–3, 2005 Feb 21, pp. 324–329.
- [19] Wahab, H. A., M. Y. Noordin, S. Izman, and D. Kurniawan. Quantitative analysis of electroplated nickel coating on hard metal. *The Scientific World Journal*, Vol. 2013, 2013 Jan 1, pp. 1–7.
- [20] Conde, A., M. A. Arenas, and J. J. De Damborenea. Electrodeposition of Zn–Ni coatings as Cd replacement for corrosion protection of high-strength steel. *Corrosion Science*, Vol. 53, No. 4, 2011 Apr 1, pp. 1489–1497.
- [21] Li, N., L. Zhang, M. Xu, T. Xia, X. Ruan, S. Song, et al. Preparation and mechanical property of electrodeposited Al-graphene composite coating. *Materials & Design*, Vol. 111, 2016 Dec 5, pp. 522–527.
- [22] Pushpavanam, M., S. R. Natarajan, K. Balakrishnan, and L. R. Sharma. Corrosion behaviour of electrodeposited zinc-nickel alloys. *Journal of Applied Electrochemistry*, Vol. 21, No. 7, 1991 Jul, pp. 642–645.

- [23] Kim, E. S., K. H. Lee, and Y. H. Moon. A feasibility study of the partial squeeze and vacuum die casting process. *Journal of Materials Processing Technology*, Vol. 105, No. 1–2, 2000 Sep 7, pp. 42–48.
- [24] Coblas, D. G., A. Fatu, A. Maoui, and M. Hajjam. Manufacturing textured surfaces: State of art and recent developments. Proceedings of the institution of mechanical engineers, Part J: Journal of Engineering Tribology, Vol. 229, No. 1, 2015 Jan, pp. 3–29.
- [25] Farooq, A., S. Ahmad, K. Hamad, and K. M. Deen. Effect of Ni concentration on the surface morphology and corrosion behavior of Zn-Ni alloy coatings. *Metals*, Vol. 12, No. 1, 2022 Jan 4, id. 96.
- [26] Vucko, F., M. Prestat, L. Holzer, B. Tribollet, K. Pélissier, and D. Thierry. Anodic degradation of Zn-Ni coatings in moderately alkaline NaCl solution. *Materials Letters*, Vol. 293, 2021 Jun 15, id. 129701.
- [27] Crasta, R. J. and S. Shetty. Comparative study of electrodeposited Zn and Zn–Ni alloy coatings for improved corrosion protection in chloride medium. *Protection of Metals and Physical Chemistry of Surfaces*, Vol. 57, No. 1, 2021 Jan, pp. 139–146.
- [28] Bae, S. H., S. Oue, I. Son, and H. Nakano. Effect of reaction product of epichlorohydrin and imidazole on the electrodeposition behavior of Zn–Ni alloy from Alkaline zincate solution. *ISIJ International*, Vol. 61, No. 8, 2021 Aug 15, pp. 2256–2263.
- [29] Kromer, R., S. Costil, C. Verdy, S. Gojon, and H. Liao. Laser surface texturing to enhance adhesion bond strength of spray coatings–Cold spraying, wire-arc spraying, and atmospheric plasma spraying. *Surface and Coatings Technology*, Vol. 352, 2018 Oct 25, pp. 642–653.
- [30] Xu, L., R. Wang, M. Gen, L. Lu, and G. Han. Preparation and properties of graphene/nickel composite coating based on the textured surface of aluminum alloy. *Materials*, Vol. 12, No. 19, 2019 Oct 3, id. 3240.
- [31] Eliaz, N., K. Venkatakrishna, and A. C. Hegde. Electroplating and characterization of Zn–Ni, Zn–Co, and Zn–Ni-Co alloys. Surface and Coatings Technology, Vol. 205, No. 7, 2010 Dec 25, pp. 1969–1978.
- [32] Dikici, T. U., O. Culha, and M. Toparli. Study of the mechanical and structural properties of Zn–Ni-Co ternary alloy electroplating. *Journal of coatings technology and research*, Vol. 7, No. 6, 2010 Nov, pp. 787–792.
- [33] Bhat, R. S. and V. B. Shet. Development and characterization of Zn–Ni, Zn–Co, and Zn–Ni-Co coatings. *Surface Engineering*, Vol. 36, No. 4, 2020 Apr 2, pp. 429–437.
- [34] American Galvanizers Association, information on web: http:// www.galvanizeit.org.
- [35] Zalnezhad, E., A. A. Sarhan, and M. Hamdi. A fuzzy logic based model to predict surface hardness of thin film TiN coating on aerospace AL7075-T6 alloy. *The International Journal of Advanced Manufacturing Technology*, Vol. 68, 2013, pp. 415–423.
- [36] Ghelichi, R., D. MacDonald, S. Bagherifard, H. Jahed, M. Guagliano, and B. Jodoin. Microstructure and fatigue behavior of cold spray coated Al5052. Acta Materialia, Vol. 60, No. 19, 2012, pp. 6555–6561.
- [37] Zalnezhad, E., A. A. Sarhan, and M. Hamdi. Optimizing the PVD TiN thin film coatings parameters on aerospace AL7075-T6 alloy for higher coating hardness and adhesion with better tribological properties of the coating surface. *The International Journal of Advanced Manufacturing Technology*, Vol. 64, 2013, pp. 281–290.
- [38] Singh, G., S. Sharma, M. Mittal, G. Singh, J. Singh, L. Changhe, et al. Impact of post-heat-treatment on the surface-roughness, residual stresses, and micromorphology characteristics of plasma-sprayed pure hydroxyapatite and 7%-Aloxite reinforced hydroxyapatite coatings deposited on titanium alloy-based biomedical implants.

- *Journal of Materials Research and Technology*, Vol. 18, 2022, pp. 1358–1380.
- [39] Singh, S. K., S. Chattopadhyaya, A. Pramanik, S. Kumar, S. M. Pandey, R. S. Walia, et al. Effect of alumina oxide nano-powder on the wear behaviour of CrN coating against cylinder liner using response surface methodology: processing and characterizations. *Journal of Materials Research and Technology*, Vol. 16, 2021, pp. 1102–1113.
- [40] Giasin, K., J. Hawxwell, J. Sinke, H. Dhakal, and U. Köklü. The effect of cutting tool coating on the form and dimensional errors of machined holes in GLARE® fibre metal laminates. *Int J Adv Manuf Technol*, Vol. 107, 2020, pp. 2817–2832.
- [41] Sharma, S., X. N. Dong, P. Wei, and C. Long. Electro-chemical deposited Cu-Ni binary and Cu-Ni-Mn ternary alloys from sulphate bath for anti-corrosive coating applications in Brine environment: Effect of Corrosion behaviour, Polarization studies, Morphological and structural characterizations. *Key Engineering Materials*, Vol. 837, pp. 102–108.
- [42] Dwivedi, S. P., S. Sharma, K. P. Sharma, A. Kumar, A. Agrawal, R. Singh, et al. The microstructure and properties of Ni-Si-La2O3 coatings deposited on 304 stainless steel by microwave cladding. *Materials*, Vol. 16, No. 6, 2023, id. 2209.
- [43] Poloczek, T., A. Lont, and J. Górka. The structure and properties of laser-cladded inconel 625/TiC composite coatings. *Materials*, Vol. 16, 2023, id. 1265.
- [44] Baghel, P. K. Effect of SMAW process parameters on similar and dissimilar metal welds: An overview. *Heliyon*, Vol. 8, No. 12, 2022 Dec 9, id. e12161. PMID: 36578398; PMCID: PMC9791349.
- [45] Kumar, S., M. Kumar, and A. Handa. High temperature oxidation and erosion-corrosion behaviour of wire arc sprayed Ni-Cr coating on boiler steel. *Materials Research Express*, Vol. 6, No. 12, 2019, id. 125533.
- [46] Al-Badra, M., M. Abd-Elhady, and H. Kandil. A novel technique for cleaning PV panels using antistatic coating with a mechanical vibrator. *Energy Reports*, Vol. 6, 2020, pp. 1633–1637.
- [47] Ganeshkumar, S., V. Thirunavukkarasu, R. Sureshkumar, S. Venkatesh, and T. Ramakrishnan. Investigation of wear behaviour of silicon carbide tool inserts and titanium nitride coated tool inserts in machining of EN8 steel. *International Journal of Mechanical Engineering and Technology*, Vol. 10, 2019, pp. 1862–1873.
- [48] Mittal, M., S. K. Nath, and S. Prakash. Effect of Al2O3 reinforcement and Al2O3–13 wt% TiO2 bond coat on plasma sprayed hydroxyapatite coating. *Defence Science Journal*, Vol. 62, 2012, pp. 193–198.
- [49] Singh, G., S. Singh, and S. Prakash. Role of post heat treatment of plasma sprayed pure and Al2O3-TiO2 reinforced hydroxyapatite coating on the microstructure and mechanical properties. *Journal* of Minerals and Materials Characterization and Engineering, Vol. 9, 2010, pp. 1059–1069.
- [50] Buchanan, V. E., P. H. Shipway, and D. G. McCartney. Microstructure and abrasive wear behaviour of shielded metal arc welding hardfacings used in the sugarcane industry. Wear, Vol. 263, 2007, pp. 99–110.
- [51] Fan, X., G. Wei, X. Lin, X. Wang, Z. Si, X. Zhang, et al. Reversible switching of interlayer exchange coupling through atomically thin VO2 via electronic state modulation. *Matter*, Vol. 2, No. 6, 2020, pp. 1582–1593.
- [52] Dai, B., B. Zhang, Z. Niu, Y. Feng, Y. Liu, and Y. Fan. A novel ultrawideband branch waveguide coupler with low amplitude imbalance. *IEEE Transactions on Microwave Theory and Techniques*, Vol. 70, 2022, pp. 3838–3846.

- [53] Feng, Y., B. Zhang, Y. Liu, Z. Niu, Y. Fan, and X. Chen. A D-band manifold triplexer with high isolation utilizing novel waveguide dual-mode filters. *In IEEE Transactions on Terahertz Science and Technology*, Vol. 12, No. 6, Nov. 2022, pp. 678–681.
- [54] Zhang, L., D. Xiong, Z. Su, J. Li, L. Yin, Z. Yao, et al. Molecular dynamics simulation and experimental study of tin growth in SAC lead-free microsolder joints under thermo-mechanical-electrical coupling. *Materials Today Communications*, Vol. 33, 2022, id. 104301.
- [55] Shi, J., B. Zhao, T. He, L. Tu, X. Lu, and H. Xu. Tribology and dynamic characteristics of textured journal-thrust coupled bearing considering thermal and pressure coupled effects. *Tribology International*, Vol. 180, 2023, id. 108292.
- [56] Zhang, P., Y. Gao, Z. Liu, S. Zhang, S. Wang, and Z. Lin. Effect of cutting parameters on the corrosion resistance of 7A04 aluminum alloy in high speed cutting. *Vacuum*, Vol. 212, 2023, id. 111968.
- [57] He, H., J. Wang, Y. Cao, X. Yang, G. Zhao, W. Yang, et al. Effect of Re and C on mechanical properties of NbTaW0.4 refractory mediumentropy alloy at elevated temperature. *Journal of Alloys and Compounds*, Vol. 931, 2023, id. 167421.
- [58] Zou, W., Y. Sun, Y. Zhou, Q. Lu, Y. Nie, T. Sun, et al. Limited sensing and deep data mining: A new exploration of developing city-wide parking guidance systems. *IEEE Intelligent Transportation Systems Magazine*, Vol. 14, No. 1, 2022, pp. 198–215.
- [59] Yang, J., L. Shang, J. Sun, S. Bai, S. Wang, J. Liu, et al. Restraining the Cr-Zr interdiffusion of Cr-coated Zr alloys in high temperature environment: A Cr/CrN/Cr coating approach. *Corrosion Science*, Vol. 214, 2023, id. 111015.
- [60] Yu, H., Y. Chen, W. Wei, X. Ji, and L. Chen. A functional organic zincchelate formation with nanoscaled granular structure enabling long-term and dendrite-free Zn anodes. *ACS Nano*, Vol. 16, No. 6, 2022, pp. 9736–9747.
- [61] Wang, H., Y. Chen, H. Yu, W. Liu, G. Kuang, L. Mei, et al. A multifunctional artificial interphase with fluorine-doped amorphous carbon layer for ultra-stable Zn anode. *Advanced Functional Materials*, Vol. 32, No. 43, 2022, id. 2205600.
- [62] Hou, X., L. Zhang, Y. Su, G. Gao, Y. Liu, Z. Na, et al. A space crawling robotic bio-paw (SCRBP) enabled by triboelectric sensors for surface identification. *Nano Energy*, Vol. 105, 2023, id. 108013.
- [63] Peng, W., S. Liu, X. Li, G. Feng, J. Xia, and Z. H. Lu. Robust hydrogen production from HCOOH over amino-modified KIT-6-confined PdIr alloy nanoparticles. *Chinese Chemical Letters*, Vol. 33, No. 3, 2022, pp. 1403–1406.
- [64] Tian, J., D. Liu, J. Li, D. Sun, H. Liu, H. Wang, et al. Cu/Cu2O nanoparticles co-regulated carbon catalyst for alkaline Al-air batteries. *Chinese Chemical Letters*, Vol. 32, No. 8, 2021, pp. 2427–2432.
- [65] Fu, Y., Q. Pan, G. Liu, and G. Zhang. Gradient structure of Ti-55531 with nano-ultrafine grains fabricated by simulation and suction casting. *Journal of Materials Engineering and Performance*, Vol. 32, No. 7, 2023, pp. 3084–3093.
- [66] Zhang, Z., J. Zhang, J. Xie, S. Liu, W. Fu, and R. Wu. Developing a Mg alloy with ultrahigh room temperature ductility via grain boundary segregation and activation of non-basal slips. *International Journal* of *Plasticity*, Vol. 162, 2023, id. 103548.
- [67] Zhang, P., Z. Liu, X. Yue, P. Wang, and Y. Zhai. Water jet impact damage mechanism and dynamic penetration energy absorption of 2A12 aluminum alloy. *Vacuum*, Vol. 206, 2022, id. 111532.
- [68] Zhang, S., B. Han, T. Zhang, Y. Chen, J. Xie, Y. Shen, et al. High-temperature solid particle erosion characteristics and damage mechanism of AlxCoCrFeNiSi high-entropy alloy coatings prepared by laser cladding. *Intermetallics*, Vol. 159, 2023, id. 107939.

- [69] Fang, J. X., J. X. Wang, Y. J. Wang, H. T. He, D. B. Zhang, and Y. Cao. Microstructure evolution and deformation behavior during stretching of a compositionally inhomogeneous TWIP-TRIP cantorlike alloy by laser powder deposition. *Materials Science and Engineering: A*, Vol. 847, 2022, id. 143319.
- [70] Zhao, D., C. Jiang, and K. Zhao. Ultrasonic welding of AZ31B magnesium alloy and pure copper: microstructure, mechanical properties and finite element analysis. *Journal of Materials Research and Technology*, Vol. 23, 2023, pp. 1273–1284.
- [71] Guo, K., G. Gou, H. Lv, and M. Shan. Jointing of CFRP/5083 aluminum alloy by induction brazing: processing, connecting mechanism, and fatigue performance. *Coatings*, Vol. 12, No. 10, 2022. id. 1559.
- [72] Fu, Z. H., B. J. Yang, M. L. Shan, T. Li, Z. Y. Zhu, C. P. Ma, et al. Hydrogen embrittlement behavior of SUS301L-MT stainless steel laser-arc hybrid welded joint localized zones. *Corrosion Science*, Vol. 164, 2020, id. 108337.
- [73] Zhu, Q., J. Chen, G. Gou, H. Chen, and P. Li. Ameliorated longitudinal critically refracted—Attenuation velocity method for welding residual stress measurement. *Journal of Materials Processing Technology*, Vol. 246, 2017, pp. 267–275.
- [74] Liao, D., S. Zhu, B. Keshtegar, G. Qian, and Q. Wang. Probabilistic framework for fatigue life assessment of notched components under size effects. *International Journal of Mechanical Sciences*, Vol. 181, 2020, id. 105685.
- [75] Niu, X., S. Zhu, J. He, D. Liao, J. A. F. O. Correia, F. Berto, et al. Defect tolerant fatique assessment of AM materials: Size effect and

- probabilistic prospects. *International Journal of Fatigue*, Vol. 160, 2022, id. 106884.
- [76] Gong, P., D. Wang, C. Zhang, Y. Wang, Z. Jamili-Shirvan, K. Yao, et al. Corrosion behavior of TiZrHfBeCu(Ni) high-entropy bulk metallic glasses in 3.5 wt. % NaCl. npj Materials Degradation, Vol. 6, 2022, id. 77.
- [77] Zhang, H., Y. Xiao, Z. Xu, M. Yang, L. Zhang, L. Yin, et al. Effects of Ni-decorated reduced graphene oxide nanosheets on the microstructural evolution and mechanical properties of Sn-3.0Ag-0.5Cu composite solders. *Intermetallics*, Vol. 150, 2022, id. 107683.
- [78] Zhang, B., Z. Wang, H. Yu, and Y. Ning. Microstructural origin and control mechanism of the mixed grain structure in Ni-based superalloys. *Journal of Alloys and Compounds*, Vol. 900, 2022, id. 163515.
- [79] Deng, H., Y. Chen, Y. Jia, Y. Pang, T. Zhang, S. Wang, et al. Microstructure and mechanical properties of dissimilar NiTi/ Ti6Al4V joints via back-heating assisted friction stir welding. *Journal of Manufacturing Processes*, Vol. 64, 2021, pp. 379–391.
- [80] Yuhua, C., M. Yuqing, L. Weiwei, and H. Peng. Investigation of welding crack in micro laser welded NiTiNb shape memory alloy and Ti6Al4V alloy dissimilar metals joints. *Optics & Laser Technology*, Vol. 91, 2017, pp. 197–202.
- [81] Chen, Y., S. Sun, T. Zhang, X. Zhou, and S. Li. Effects of post-weld heat treatment on the microstructure and mechanical properties of laser-welded NiTi/304SS joint with Ni filler. *Materials Science and Engineering: A*, Vol. 771, 2020, id. 138545.